Application of X-rays to Interpret Intensity Ratios for Nickel in Nickel (II) Oxide

O.K. Köksal[a,b], Ö. Söğüt[c,*], E. Küçükönder[d] and S. Dağli[e]

[a] *Adıyaman University, Faculty of Engineering, Department of Electrical and Electronics Engineering, 02040, Adıyaman, Türkiye*
[b] *Karadeniz Technical University, Faculty of Science, Department of Physics, 61080, Trabzon, Türkiye*
[c] *Kahramanmaraş Sutcu Imam University, Faculty of Science and Letters, Department of Physics, 46100, Kahramanmaraş, Türkiye*
[d] *Kahramanmaraş Sütçü İmam University, Vocational School of Technical Sciences, Department of Materials and Materials Processing Technologies, 46100, Kahramanmaş, Türkiye*
[e] *İbni Sina Vocational Technical and Anatolian High School, 01250, Sarıçam, Adana, Türkiye*

Received: 02.11.2022 & Accepted: 24.02.2023

Doi: 10.12693/APhysPolA.143.362 *e-mail: omersogut@gmail.com

The K-shell characteristic X-ray intensity ratios of nickel (II) oxide thin films generated by chemical spraying with 1–6 percent boron doping were studied. An americium-241 radioisotope source generated 59.543 kilo-electron volt gamma rays at 50 mili Curie intensity for these samples. The distinctive X-rays of the samples were calculated using a Canberra ultra-low energy germanium detector (with a resolution of 150 electron volts at 5.96 keV). The results were interpreted based on the amount of boron doped in nickel (II) oxide thin films, and it was discovered that, with the exception of boron doping quantities of 5 percent and 6 percent, K-shell X-ray intensity ratios rose as boron doping amounts increased. The findings are given and compared to those of the previous study. The obtained results are provided and compared in the table to the other researchers' theoretical and experimental results.

topics: NiO, boron, K-shell intensity ratio, thin film

1. Introduction

Nickel oxide (NiO) is a p-type semiconducting oxide material with a large band gap of from 3.6 to 4 eV that is widely utilized as an antiferromagnetic layer, a functional sensor layer in chemical sensors, and an active layer in electrochromic devices [1]. NiO thin films have also been investigated as a desirable material for electrochromic devices and as a functional sensor layer for gas sensors [2–5]. NiO was once thought to be a prototypical hole-type semiconductor. Because the chemical stability of the layers, as well as their optical and electrical properties, have been outstanding, these films have been created using a variety of physical and chemical vapor deposition processes, such as reactive sputtering and plasma-enhanced chemical vapor deposition. The relationship between film characteristics and process parameters, however, is poorly understood. For example, chemical bath deposition [6], reactive sputtering [7], electron beam evaporation [8], spray pyrolysis [9], plasma accelerated chemical vapor deposition [10], pulsed laser deposition [11], DC reactive magnetron [3] etc., and many of their features were investigated.

With the increasing complexity of materials used in industrial and scientific settings, the energy-dispersive X-ray fluorescence (EDXRF) approach has been widely employed for qualitative and quantitative analysis of elements and compounds in a sample, gaining more significance in the examination of these materials' physical and chemical properties [12]. In investigation [13], the average L-shell fluorescence efficiencies and L_3-subshell fluorescence efficiencies for the elements and their compounds in the $73 \leq Z \leq 78$ atom area were estimated. The purpose of work [14] was to define the impact of chemistry and multiple ionization on the L-shell production cross-sections, X-ray intensity ratios, and average L-shell fluorescence yields of both pure Ta and W elements and their compounds (Ta, $TaCl_5$, TaF_5, TaI_5, W, WS_2, WSi_2, W_2B_5, WC, WO_3, $Na_2WO_42H_2O$, WCl_6). In study [15], L-shell production cross-section values Li, an intensity ratio value $I_{Lj}/I_{L_\alpha 1,2}$, and L-subshell fluorescence yield values of elements with atomic numbers between 50 and 92 have been examined. The study presented in [16] experimentally established K-shell fluorescence characteristics for elements with atomic numbers Z ranging from 21 to 30.

The K- and L-shell X-ray fluorescence properties of Co, Cu, and Ag in pure metals and in various alloy compositions were measured in [17]. Work [18] compared experimental and theoretical values to examine the alloying influence on K_β/K_α X-ray intensity ratios, K X-ray generation cross-sections, fluorescence yields, and $KLM/K_{1,2}$ and $KMM/K_{1,3}$ radiative Auger ratios in Zn_xCo_{1-x} alloys relative to the pure metal for different concentrations. In study [19], the valence electronic structure of Ni in Ni–B alloy coatings has been determined using the K-to-K intensity ratio, and the differences in the 3D electron population between pure Ni and alloys have been used to analyze why there is an inconsistency between them. As is clear from earlier investigations, the X-ray fluorescence technique has been used for a wide range of pure elements and compounds, and a number of effects that have an impact on the fluorescence characteristics have been identified.

By oxidizing the p-type NiO layer, research on transparent ohmic contacts for boron-doped diamond has been conducted [20]. Another work [21] investigated the synthesis and characterization of spray pyrolyzed boron-doped NiO thin films. Additionally, the optical characteristics of NiO thin films with nanoscale boron doping were examined [22]. Sol–gel-produced Al-doped B-substituted NiO films' electrochromic characteristics were also investigated [23]. It is clear from all of that research that the properties of boron-doped NiO samples, including contact structure, synthesis, characterization, optics, and electrochromic properties, were examined.

In this study, the X-ray fluorescence technique (XRF) was used to detect K_β/K_α characteristic X-ray intensity ratios, and the focus was on the changes in K_β/K_α characteristic X-ray intensity ratios of boron-doped NiO thin films as boron doping quantities increased.

Numerous features of the NiO compound, which plays a significant role in the field of materials, have been revealed in previous studies, but the valence electron structure has not been the subject of any research. The results of the K-shell intensity ratio utilized to comprehend the valence electron density are presented in this paper. In this regard, the study has remedied the existing shortcoming. It is anticipated that this research will pave the way for future research on valence electron structures.

2. Experimental procedure

2.1. Preparation of sample

By airbrush spraying, B-doped NiO thin films were created on glass substrates. A basic NiO solution was produced by dissolving 0.1 M nickel nitrate hexahydrate ($Ni(NO_3)_26H_2O$) in distilled water. In order to dope the base solution, 0.1 M boric acid (H3BO3) was dissolved in distilled water and added in the proper atomic ratio. Changing the B content (1–6 at.%) changed the atomic ratios of B/NiO in the solution. Using a pressurized airbrush spray, the starting solution was sprayed onto heated surfaces at 400°C. The precursor solution was deposited cyclically, with 8 s of spraying followed by 50 s without spraying, to maintain the substrate temperature constant. The airbrush's lateral speed was set at 1 cm/s, the spray nozzle to substrate distance was adjusted to 35 cm, and the air pressure was adjusted to set the volumetric spray rate at roughly 0.3 mL/s in order to achieve a uniform layer thickness. There were 20 repetitions of spraying required to create films with a thickness of roughly 1 m. Looking at the X-ray diffraction (XRD) results, it is seen that no peaks other than leading impurities such as boron or nickel metals and their compounds are observed in the samples [21].

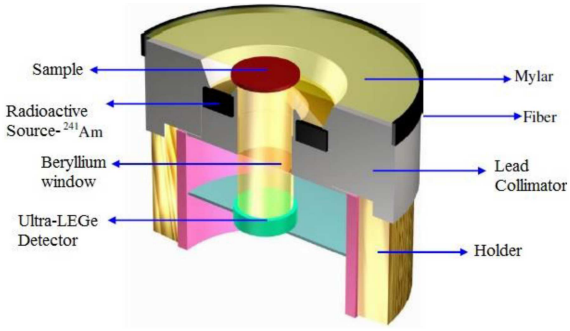

Fig. 1. Experimental geometries used to obtain emission spectra with 50 mCi Am-241 source.

2.2. Detection of K_β and K_α X-rays

Gamma rays emanating from the Am-241 radioisotope source at 50 mCi intensity were used to excite the NiO:B thin film samples. The calculation of the characteristic X-rays emitted from the materials was done with a Canberra Ultra-LEGe detector (FWHM = 155 eV at 5.96 keV, active area = 30 mm^2, thickness = 5 mm, polymer window thickness = 0.4 mm). To reduce the number of inaccuracies caused by the counting statistic, each sample was calculated with an actual calculation time of at least 5000 s (live time). Figure 1 shows a schematic representation of the experiment geometry for calculating the K_β and K_α X-rays of the produced samples.

Using the following relation, the K_β/K_α X-ray intensity ratio values were computed,

$$\frac{I_{K_\beta}}{I_{K_\alpha}} = \frac{N_{K_\beta}}{N_{K_\alpha}} \frac{I_0 G\, \varepsilon_{K_\alpha}}{I_0 G\, \varepsilon_{K_\beta}} \frac{\beta_{K_\alpha}}{\beta_{K_\beta}}. \quad (1)$$

Here, N_{K_β} and N_{K_α} are target self-absorption correction factors for both incident and emitted radiation, while ε_{K_β} and ε_{K_α} are detector efficiencies

TABLE I

The empirical and theoretical values of K-Shell X-ray intensity ratios of current samples at 59.54 keV.

Sample	Boron doping [%]	Exper.	Theor.				
		I_{K_β}/I_{K_α}	Scofield 1974 [25]	Scofield 1974 [26]	Electronic configuration	Coulomb gauge [27]	Babushkin gauge [27]
Pure nickel	0	0.1376 ± 0.0083	0.1227	0.1401	$3d^6 4s^2 4p^2$	0.1439	0.1452
					$3d^7 4s^2 4p^1$	0.1397	0.1410
					$3d^8 4s^2$	0.1361	0.1374
					$3d^9 4s^1$	0.1333	0.1346
					$3d^{10}$	0.1313	0.1325
NiO	0	0.1089 ± 0.0065	–	–	–	–	–
NiO:B	1	0.1162 ± 0.0070	–	–	–	–	–
NiO:B	2	0.1147 ± 0.0069	–	–	–	–	–
NiO:B	3	0.1221 ± 0.0073	–	–	–	–	–
NiO:B	4	0.1223 ± 0.0073	–	–	–	–	–
NiO:B	5	0.1178 ± 0.0071	–	–	–	–	–
NiO:B	6	0.1189 ± 0.0071	–	–	–	–	–

for K_β and K_α X-rays, respectively. In (1), G is a geometrical factor, and I_0 is the intensity of the incident radiation. The detector efficiency of the $I_0 G\varepsilon$ values is often calculated in a separate experiment in experimental research. The values $I_0 G\varepsilon$, which include terms related to the incident photons, geometrical factor, and the absolute efficiency of the X-ray detector in the examined energy range in the same geometry, were calculated using the K_β and K_α characteristic with X-rays of the elements in the $24 \leq Z \leq 48$ range. The relationship determined the values $I_0 G\varepsilon$ for the current configuration

$$I_0 G\varepsilon = \frac{N_{K_i}}{\sigma_{K_i}\beta_{K_i}\, t}, \tag{2}$$

with $i = \alpha, \beta$, where N_{Ki} represents the number of K_α and K_β X-rays recorded at the K_α and K_β peaks, and σ_{K_i} represents the σ_{K_α} or σ_{K_β} K-shell fluorescence cross-section. Using the formulae for Am-241, the value of $I_0 G\varepsilon$ was fit as a function of energy accordingly

$$I_0 G\,\varepsilon_{K_i} = A_0 + A_1 E_i + A_2 E_i^2 + A_3 E_i^3 + B_0 + B_1 E_i + B_2 E_i^2, \tag{3}$$

where E_i is the X-ray energy of type K_α or K_β. The experimental efficiency curve for the ultra-low energy germanium detector is plotted as a function of K X-ray energy. The left and right sides of experimental efficiency curve are represented by (3) in the investigation [24].

The self-absorption correction factor for K_α and K_β was determined individually using

$$C_k = \frac{1 - \left[-\left(\frac{\mu_p}{\cos(\theta)} + \frac{\mu_e}{\cos(\varphi)} \right) t \right]}{\left(\frac{\mu_p}{\cos(\theta)} + \frac{\mu_e}{\cos(\varphi)} \right) t}, \tag{4}$$

where the mass attenuation coefficients at the incident photon energy and emitted characteristic X-rays of the sample are μ_{inc} [cm^2/g] and μ_e [cm^2/g], respectively. The measured mass thickness of the sample is t [g/cm^2].

3. Results and discussion

Table I (see also [25–27]) shows the K_β/K_α X-ray intensity ratios of pure Ni, boron-undoped NiO thin film, and NiO thin film made by chemical spraying with a 1–6% boron addition.

Figure 2 shows the spectral responses of boron-undoped and boron-doped NiO thin films activated with an Am-241 radioisotope source. According to Fig. 2, there is no change in the energy of the nickel peak, which means that the measurement system is effective in this regard. In addition to the nickel peaks K_α and K_β, two more peaks are seen in the spectrum. These peaks are a part of the lead plate L_α and L_β peaks, which protect the system. The peak heights and net areas of Ni in boron-undoped NiO and 1–6% boron-doped NiO thin films are very different, as shown in Fig. 3.

Chemical effects on the K X-ray intensity ratios could be to blame for the discrepancies in peaks because the X-ray lines emitted by a pure element differ from those emitted by the same element in a chemical structure. Additionally, theoretical and practical K_β/K_α X-ray intensity ratios for pure Ni, boron-undoped NiO, and boron-doped NiO thin films have been examined in [25, 26, 28] and other experimental results are presented in [29–34].

As seen in Table I, current experimental values for pure Ni differ by 9% and 24%, respectively, from theoretical values [25, 26]. The changes in K_β/K_α X-ray intensity ratios of boron-doped NiO thin films

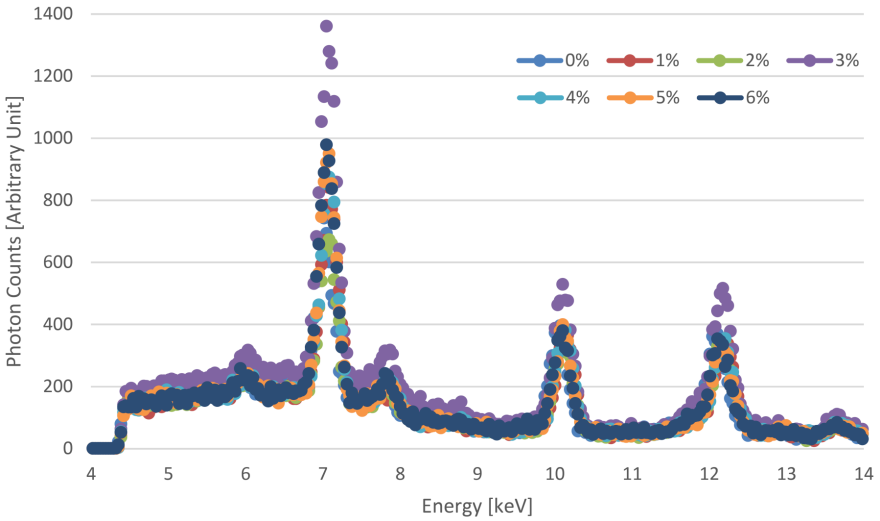

Fig. 2. The spectra of boron-undoped and 1–6% boron-doped nickel (II) oxide thin films stimulated with an americium-241 radioisotope.

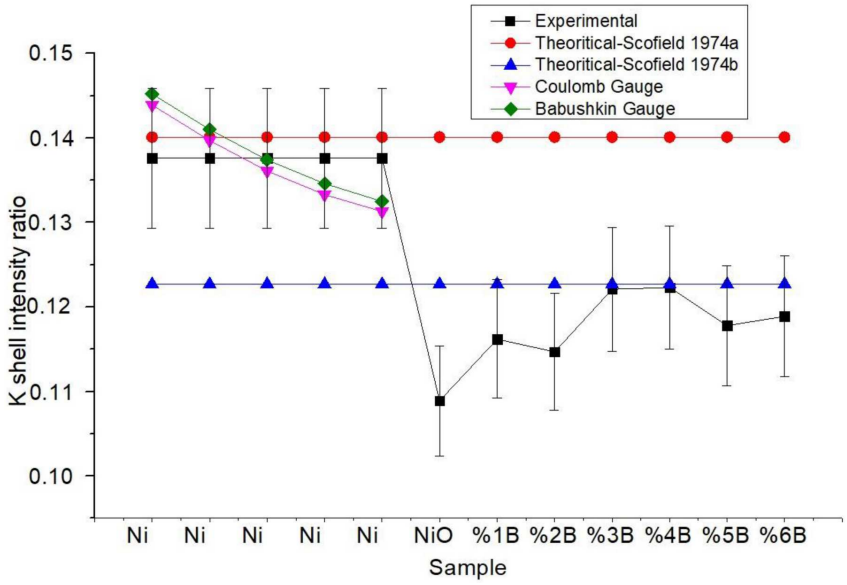

Fig. 3. The change of K-shell X-ray intensity rates measured by Canberra ultra-low energy germanium detector according to the boron doping amounts.

TABLE II

Inaccuracies in the numbers used to calculate the parameters.

Quality	Nature of uncertainty	Uncertainty [%]
N_{Ki} $(i=\alpha,\beta)$	peak area's assessment	≤ 2
$I_0 G\,\varepsilon_{Ki}$	many criteria are used to evaluate the component	≤ 3
β	correction factor for absorption	≤ 3
t	object thickness	≤ 2

are found to be 0.3–7% and 15–22%, respectively, when compared to theoretical values [25, 26]. They differ by 20–26 percent when compared to experimental results from [29]. However, the K_β/K_α X-ray intensity ratios of the boron-doped NiO thin film deviate by 2–6% and 5–11% from those of pure Ni and boron-undoped NiO thin films, respectively. The margins of error in the calculations are shown in Table II.

When examining Fig. 3, it can be seen that K-shell X-ray intensity ratio values of pure nickel are compatible with those in [26] and Coulomb and Babushkin approaches [27], whereas NiO:B thin films are compatible with the approach presented in [55].

Boron doping in NiO thin films altered K_β and K_α X-ray emission capabilities of Ni (as seen in Fig. 2). When compared to other experimental and theoretical values, the experimental K_β/K_α X-ray intensity ratios of boron-doped NiO thin films vary by 10–26% and 0.3–18%, respectively. As a result, it can be concluded that the chemical structure of the materials has an impact on K_β/K_α X-ray intensity ratios. Specifically, unlike in the pure element state, when an element enters the structure of an alloy, a chemical compound, or a thin film, it affects the energy, wavelength, and shape of the emitted X-ray line.

The electron configuration of Ni is [Ar] $3d^8 4s^2$, and its valence state is $3d$. The vacancy in the K-shell is filled by some of the N- or M-subshells, which results in some K_β X-rays. As a result, K_β transitions are unaffected by valence state, although they are affected by an element's or compound's valence state fluctuation. Furthermore, the valence electron configurations of a compounded element and its pure form are distinct. In addition, further experimental and theoretical data are required to verify the validity of the results presented.

In order to identify experimental uncertainty, measurements were repeated for each sample, with a magnetic field value, without a sample, and without a magnetic field. Throughout the experiment, all components of the system remained stable. In this study, the experimental uncertainty was calculated using the equation

$$\text{uncertainity of the cross sec.} = \text{exp. result} \sqrt{\left(\frac{\Delta N}{N}\right)^2 + \left(\frac{\Delta I_0 G\varepsilon}{I_0 G\varepsilon}\right)^2 + \left(\frac{\Delta t}{t}\right)^2 + \left(\frac{\Delta\beta}{\beta}\right)^2}, \tag{5}$$

where ΔN_{K_β} and ΔN_{K_α} are calculation uncertainty of the peaks of the K_β and K_α X-ray intensity, $\Delta\beta_{K_\beta}$ and $\Delta\beta_{K_\alpha}$ are β_{K_i} uncertainty for the K_β and K_α X-ray photons, and $\Delta I_0 G\varepsilon_{K_\alpha}$ and $\Delta I_0 G\varepsilon_{K_\beta}$ are effective photon flux uncertainty at the K_β and K_α energies. The overall degree of uncertainty (approximately 6%) in several aspects was calculated including peak area evaluation (2%), $I_0 G\varepsilon_{Ki}$ product (3%), absorption correction factor (3%), and object thickness (2%).

It can be shown that the pure nickel K-shell intensity ratio measurements are consistent with the theoretical values. It is evident that several values for the boron-doped NiO compound at different concentrations do not match the theoretical values. This is because, in the absence of theoretical equivalents, these created samples are contrasted with pure nickel.

4. Conclusions

In this study, the effects of boron doping of NiO thin films from 1 to 6% on the K_β/K_α X-ray intensity ratios of nickel within NiO thin films were examined. It can be argued that doping boron into NiO thin film increases the probability of K_β X-ray emission by changing the valence state of Ni present in the structure of NiO thin film. Note that K_β/K_α X-ray intensity rates increased as the amount of boron doped into NiO thin films increased.

The energy dispersive X-ray fluorescence (EDXRF) technique is highly useful for determining the K_β/K_α X-ray intensity ratios, as evidenced by this and another research. We feel that the findings of this study will be valuable in a variety of research areas, such as electrochromic devices and a functioning sensor layer for gas sensors, among others.

Due to the transverse (Breit) interaction, self-energy, and vacuum polarization adjustments, the obtained K-shell X-ray intensity ratios of pure nickel are suitable Babushkin and Coulomb values [27] and agree quite well with estimated [26] values of the ratios of the K X-ray components, which are in good agreement with the experimental data in contrast to the earlier single potential calculations because of the exchange corrections of K X-ray emission rates.

The derived K-shell intensity ratios of NiO:B (1%, 2%, 3%, 4%, 5%, 6%) have been seen to vary from Babushkin and Coulomb values [27] due to the transverse (Breit) interaction, self-energy, and vacuum polarization adjustments, and agree quite well with values in [25], depending on how the single-electron functions are constructed and the gauge convention used. Depending on how single-electron functions are generated and the tuning convention chosen, it is possible to say that the transverse (Breit) interaction, self-energy, and vacuum polarization corrections have no impact on the samples created using the chemical spray approach [35].

In a previous work using the same materials as this one [21], it was discovered that spray pyrolysis-produced NiO thin films were affected by B doping. Other than precursor impurities like B or Ni metals and their compounds, no peaks were seen. The cubic structure of the NiO films is not altered by B doping, as shown by the XRD patterns, and the intensity of the (111), (200), and (220) peaks increase almost linearly with increasing boron concentration. When the boron impurity enters the NiO matrix, a shift in the (111) and (200) peaks is noticed, suggesting that the films still contain some residual stress. Situations in the sample fabrication

process are among our error causes, in addition to measurement mistake and inaccuracies from comparison with pure nickel.

The valence electron state of pure nickel is identical to $3d^8 4s^2$, however, when oxygen and boron are added at different quantities, it is important to consider the non-rearrangement between the $3d$ and $4s4p$ states [27, 36]. Considering all the above remarks, it should be noted that the accuracy of the boron doping ratios in the sample production process is not complete.

The obtained results made it possible to reliably interpret different experimental K_β-to-K_α X-ray intensity ratios for $3d$ transition metals in their compounds and alloys. They can also give quantitative data about changes in the valence electronic configurations of these metals in the systems under consideration.

Acknowledgments

The authors prepared the samples used in this study in the Thin Film Laboratory of the Department of Physics at KSU. We thank Prof. Dr. Ümit Alver and Dr. Hakan Yaykaşlıfor providing us with the samples. We also thank Karadeniz Technical University Spectroscopy Laboratory for the X-ray fluorescence measurements.

References

[1] S. Sriram, A. Thayumanavan, *Int. J. Mater. Sci. Eng.* **1**, 118 (2013).

[2] J.W. Lee, I.H. Park, C.W. Chung, *Integr. Ferroelectr.* **74**, 71 (2005).

[3] I. Hotovy, J. Huran, P. Siciliano, S. Capone, L. Spiess, V. Rehacek, *Sens. Actuators B Chem.* **78**, 126 (2001).

[4] M. Kitao, K. Izawa, K. Urabe, T. Komatsu, S. Kuwano, S. Yamada, *Jpn. J. Appl. Phys.* **33**, 6656 (1994).

[5] K. Yoshimura, T. Miki, S. Tanemura, *Jpn. J. Appl. Phys.* **34**, 2440 (1995).

[6] X. Xia, J. Tu, J. Zhang, X.L. Wang, W.K. Zhang, H. Huang, *Sol. Energy Mater. Sol. Cells* **92**, 628 (2008).

[7] I. Hotový, D. Búc, Š. Haščík, O. Nennewitz, *Vacuum* **50**, 41 (1998).

[8] D.Y. Jiang, J.M. Qin, X. Wang, S. Gao, Q.C. Liang, J.X. Zhao, *Vacuum* **86**, 1083 (2012).

[9] L. Cattin, B.A. Reguig, A. Khelil, M. Morsli, K. Benchouk, J. Bernède, *Appl. Surf. Sci.* **254**, 5814 (2008).

[10] E. Fujii, A. Tomozawa, H. Torii, R. Takayama, *Jpn. J. Appl. Phys.* **35**, L328 (1996).

[11] I. Fasaki, A. Koutoulaki, M. Kompitsas, C. Charitidis, *Appl. Surf. Sci.* **257**, 429 (2010).

[12] R. Unterumsberger, P. Hönicke, B. Pollakowski-Herrmann, M. Müller, B. Beckhoff, *Spectrochim. Acta B: At. Spectrosc.* **145**, 71 (2018).

[13] E. Cengiz, E. Tıraşoğlu, V. Aylıkcı, G. Apaydın, N.K. Aylıkcı, *Chem. Phys. Lett.* **498**, 107 (2010).

[14] C. Aksoy, E. Tıraşoğlu, E. Cengiz, G. Apaydın, M. Saydam, V. Aylıkçı, N. Aylıkçı, *J. Electron Spectrosc. Relat. Phenom.* **184**, 556 (2012).

[15] V. Aylikci, A. Kahoul, N.K. Aylikci, E. Tiraşoğlu, İ.H. Karahan, A. Abassi, M. Dogan, *Radiat. Phys. Chem.* **106**, 99 (2015).

[16] V. Aylikci, A. Kahoul, N.K. Aylikci, E. Tiraşoğlu, İ.H. Karahan, *Spectrosc. Lett.* **48**, 331 (2015).

[17] N.K. Aylikci, E. Tiraşoğlu, G. Apaydin, E. Cengiz, V. Aylikci, Ö.F. Bakkaloğlu, *Chem. Phys. Lett.* **475**, 135 (2009).

[18] N.K. Aylikci, E. Tiraşoğlu, İ.H. Karahan, V. Aylikci, E. Cengiz, G. Apaydin, *Chem. Phys. Lett.* **484**, 368 (2010).

[19] E. Cengiz, O.K. Köksal, G. Apaydın, İ.H. Karahan, E. Ünal, *Appl. Radiat. Isot.* **144**, 24 (2019).

[20] T. Zhang, X. Li, T. Pu, Q. Wang, S. Cheng, L. Li, *Mater. Sci. Semicond. Process.* **105**, 104740 (2020).

[21] U. Alver, H. Yaykaşlı, S. Kerli, A. Tanrıverdi, *Int. J. Miner. Metall. Mater.* **20**, 1097 (2013).

[22] H. Aydin, S.A. Mansour, C. Aydin, A.A. Al-Ghamdi, O.A. Al-Hartomy, F. El-Tantawy, F. Yakuphanoglu, *J. Sol-Gel Sci. Technol.* **64**, 728 (2012).

[23] X. Lou, X. Zhao, J. Feng, X. Zhou, *Prog. Org. Coat.* **64**, 300 (2009).

[24] E. Cengiz, E. Tıraşoğlu, G. Apaydın, O.K. Köksal, *Spectrosc. Lett.* **54**, 274 (2021).

[25] J.H. Scofield, *At. Data Nucl. Data Tables* **14**, 121 (1974).

[26] J.H. Scofield, *Phys. Rev. A* **9**, 1041 (1974).

[27] S. Raj, H.C. Padhi, P. Palit, D.K. Basa, M. Polasik, F. Pawłowski, *Phys. Rev. B* **65**, 193105 (2002).

[28] S.I. Salem, S.L. Panossian, R.A. Krause, *At. Data Nucl. Data Tables* **14**, 91 (1974).

[29] O. Sogut, E. Büyükkasap, H. Erdoğan, *Radiat. Phys. Chem.* **64**, 343 (2002).

[30] M.R. Khan, M. Karimi, *X-Ray Spectrom.* **9**, 32 (1980).

[31] N.V. Rao, S.B. Reddy, G. Satyanarayana, D.L. Sastry, *Physica B+C* **138**, 215 (1986).

[32] L. Rebohle, U. Lehnert, G. Zschornack, *X-Ray Spectrom.* **25**, 295 (1996).

[33] S.T. Manson, D.J. Kennedy, *At. Data Nucl. Data Tables* **14**, 111 (1974).

[34] M. Ertugrul, Ö. Sögüt, Ö. Simsek, E. Büyükkasap, *J. Phys. B: At. Mol. Opt. Phys.* **34**, 909 (2001).

[35] K. Jankowski, M. Polasik, *J. Phys. B: At. Mol. Opt. Phys.* **22**, 2369 (1989).

[36] F. Pawłowski, M. Polasik, S. Raj, H.C. Padhi, D.K. Basa, *Nucl. Instrum. Methods Phys. Res. B* **195**, 367 (2002).